

Indirect Detection Signatures for the Origin of Asymmetric Dark Matter

Yue Zhao¹ and Kathryn M. Zurek²

¹*Stanford Institute of Theoretical Physics, Physics Department,
Stanford University, Stanford, CA 94305, USA*

²*Michigan Center for Theoretical Physics,
University of Michigan, Ann Arbor, MI 48109, USA*

Abstract

We study the decay signatures of Asymmetric Dark Matter (ADM) via higher dimension operators which are responsible for generating the primordial dark matter (DM) asymmetry. Since the signatures are sensitive both to the nature of the higher dimension operator generating the DM asymmetry and to the sign of the baryon or lepton number that the DM carries, indirect detection may provide a window into the nature of the mechanism which generates the DM asymmetry. We consider in particular dimension-6 fermionic operators of the form $\mathcal{O}_{ADM} = X\mathcal{O}_{B-L}/M^2$, where $\mathcal{O}_{B-L} = u^c d^c d^c, \ell \ell e^c, q \ell d^c$ (or operators related through a Hermitian conjugate) with the scale M around or just below the GUT scale. We derive constraints on ADM particles both in the natural mass range (around a few GeV), as well as in the range between 100 GeV to 10 TeV. For light ADM, we focus on constraints from both the low energy gamma ray data and proton/anti-proton fluxes. For heavy ADM, we consider γ -rays and proton/anti-proton fluxes, and we fit e^+/e^- data from AMS-02 and H.E.S.S. (neglecting the Fermi charged particle fluxes which disagree with AMS-02 below 100 GeV). We show that, although the best fit regions from electron/positron measurement are still in tension with other channels on account of the H.E.S.S. measurement at high energies, compared to an ordinary symmetric dark matter scenario, the decay of DM with a primordial asymmetry reduces the tension. Better measurement of the flux at high energy will be necessary to draw a definite conclusion about the viability of decaying DM as source for the signals.

Contents

I. Introduction	2
II. Operators for Asymmetric Dark Matter Decay	7
III. Photons from Dark Matter Decay	9
A. Photon Flux from DM Decay	10
1. Galactic DM Halo	10
2. Extra-galactic γ -ray	11
B. Data and Statistical Methodology	13
IV. Charged Particles From Dark Matter Decay	14
1. e^+/e^- Fit from AMS-02 and H.E.S.S.	15
2. Constraints from p^+/p^- Fluxes	17
V. Constraints on ADM decay	20
A. Light ADM Scenario	20
B. Heavy ADM scenario	21
VI. Conclusions	27
Acknowledgments	28
A. A Toy Model for Heavy ADM	28
References	30

I. INTRODUCTION

Asymmetric Dark Matter (ADM) is a compelling alternative to WIMP models of dark matter (DM) with thermal freeze-out. In these models the DM density is set by its particle-anti-particle asymmetry, similar to the baryon asymmetry, rather than by its annihilation cross-section.

While the idea that DM may carry a particle asymmetry has existed in the literature for a long time [1–8], it has only been relatively recently that robust classes of models based on higher dimension operators were introduced [9].

The ADM operators communicate an asymmetry between the DM and visible sectors, and have the advantage that they naturally decouple at low energies, leading to conserved baryon and DM asymmetries separately in the two sectors late in the Universe. These operators take on the form

$$\mathcal{O}_{ADM} = \frac{\mathcal{O}_{B-L}\mathcal{O}_X}{M^{n+m-4}}, \quad (1)$$

where \mathcal{O}_{B-L} has dimension m and \mathcal{O}_X has dimension n . By sharing a primordial asymmetry between the two sectors, the models naturally realize the relationship $n_X - n_{\bar{X}} \sim n_b - n_{\bar{b}}$. Since the observed baryon to DM energy density is $\rho_{DM}/\rho_b \sim 5$, this implies the natural mass scale of ADM is ~ 5 GeV.¹ For a review and list of references of DM models employing higher dimension operators, see [10].

As outlined in [10], for such higher-dimension ADM models, there are two basic categories of models. In the first class a primordial matter anti-matter asymmetry is shared between the DM and visible sectors via interactions that are mediated by heavy particles that become integrated out as the temperature of the Universe drops [12–16]. Such scenarios give rise to DM particles whose relic abundance carries the same baryon or lepton number as visible particles. The second category generates opposite charge asymmetries for the SM and DM sectors via non-equilibrium processes [17–32]. In this case, the DM particles naturally carry opposite baryon/lepton numbers relative to SM particles in our Universe.

Examples of operators which may transfer an asymmetry between sectors are

$$\mathcal{O}_{B-L} = LH, \quad U^c D^c D^c, \quad QLD^c, \quad LLE^c, \quad (2)$$

where L is the chiral supermultiplet of a SM lepton doublet, H is the Higgs doublet, U^c , D^c are right-handed anti-quarks, E^c is a right-handed charged anti-lepton, and Q is a quark doublet. In

¹ The DM may, however, be heavier if new X -violating interactions are present to deplete the X -asymmetry in comparison to the baryon asymmetry. We discuss this case further below.

the context of supersymmetry, these operators are R -parity violating, and having the simplest interaction with the DM X , the simplest ADM interactions take the form

$$W_{\text{ADM}} = XLH, \quad \frac{XU_i^c D_j^c D_k^c}{M_{ijk}}, \quad \frac{XQ_i L_j D_k^c}{M_{ijk}}, \quad \frac{XL_i L_j E_k^c}{M_{ijk}}, \quad (3)$$

where now we have explicitly included a flavor index i, j, k on the generic scale of the operator M .

In the context of supersymmetry, the ADM particle is stabilized by R -parity. On the other hand, the analogue fermionic operators, of the form²

$$\mathcal{O}_{\text{ADM}} = X\ell H, \quad \frac{Xu_i^c d_j^c d_k^c}{M_{ijk}^2}, \quad \frac{Xq_i \ell_j d_k^c}{M_{ijk}^2}, \quad \frac{X\ell_i \ell_j e_k^c}{M_{ijk}^2}, \quad (4)$$

may also share a primordial between the two sectors. To distinguish from superpotential multiplets in SUSY, we use lower case letters for the SM fermionic fields in the Lagrangian, and to label the operator conveniently, we use the SM part of the operator as a subscript. For example, we label $\frac{Xu_i^c d_j^c d_k^c}{M_{ijk}^2}$ as \mathcal{O}_{UDD} . When working with a non-holomorphic Lagrangian, instead of a superpotential, many more possibilities arise, such as

$$\mathcal{O}_{\text{ADM}} = \frac{Xd_i^c u_j^{c\dagger} e_k^{c\dagger}}{M_{ijk}^2}, \quad \frac{Xq_i \ell_j^\dagger u_k^c}{M_{ijk}^2}, \quad \frac{Xq_i d_j^{c\dagger} q_k}{M_{ijk}^2}. \quad (5)$$

The effective baryon or lepton number of the DM (which is defined as being opposite of the $B - L$ charge carried by \mathcal{O}_{B-L}) in each of the operators differs. Both types of operators may be easily UV completed, and the flavor structure depends on the UV completion. For example, $\frac{X\ell_i \ell_j e_k^c}{M_{ijk}^2}$ can be obtained by the Lagrangian $\mathcal{L} \supset y_i X \ell_i \Phi + y'_{jk} \Phi^\dagger \ell_j e_k^c$, where $i, j, k = 1, 2, 3$ for 3 generations and Φ is a heavy scalar field in fundamental representation of $SU(2)_W$. If $y_i = y'_{jk}$ for all i, j and k , we obtain a universal flavor structure for $\frac{X\ell_i \ell_j e_k^c}{M_{ijk}^2}$.³

² We do not include other choices of Lorentz structures for these 4-fermion interactions since they do not make a substantial difference in the indirect detection signals.

³ We emphasize that one can UV complete this operator in another way, i.e. $\mathcal{L} \supset y_{1,i} X e_i^c \Phi + y_{2,jk} \Phi^\dagger \ell_j \ell_k$. In this case, Φ is a heavy scalar field but a singlet in $SU(2)_W$. Since ℓ_j and ℓ_k have to contract by an anti-symmetric tensor in the $SU(2)_W$ basis, they must be in different generations. A similar subtlety also occurs for the $\frac{Xu_i^c d_j^c d_k^c}{M_{ijk}^2}$ operator.

While these operators induce an asymmetry in the two sectors, they also cause the fermionic X to decay. If its abundance has not been cosmologically depleted in the early Universe, and M is a high scale, the decay lifetime can be long. Assuming the heavy mediator is a scalar field, *i.e.* in the form of the effective operators in Eq. (4), the decay lifetime is approximately

$$c\tau \simeq \frac{6144\pi^3 M^4}{C_{color} C_{flavor} C_{SU(2)_W} m_X^5} \simeq 3.9 \times 10^{26} \text{ s} \left(\frac{M}{10^{13} \text{ GeV}}\right)^4 \left(\frac{20 \text{ GeV}}{m_X}\right)^5 \frac{1}{C_{color}} \frac{1}{C_{flavor}} \frac{1}{C_{SU(2)_W}}. \quad (6)$$

Here C_{color} , C_{flavor} and $C_{SU(2)_W}$ indicate the constants introduced from color, flavor and weak isospin combinations in the final states.

Observations of the DM decay products in high energy gamma rays and in charged particles (electrons, positrons and anti-protons) thus will constrain M . As we will show, if $M \gtrsim 10^{13}$ GeV, these lifetimes are on the order of current constraints, and their decay may be detectable both in photons and in charged cosmic ray byproducts. Similar decay signatures have also been studied in many other contexts. (Please see [33] and the references therein for a review.) As pointed out in [34, 35], current constraints from indirect detection implies a suppression scale around the GUT scale if weak scale DM decays through dimension 6 operators. Most studies, however, have mainly focused on symmetric DM. In this paper, we focus on the asymmetric DM scenario, and, as we will see, the sign of the effective DM baryon or lepton number substantially affects the results. Refs. [35–40] also studied scenarios where DM particles decay asymmetrically. In these studies, however, the operators which induce DM decay may not be those which are responsible for generating the asymmetry in DM sector as in ordinary ADM models. In Ref. [41], the authors briefly mentioned the possibility of ADM decay induced by the operators in ordinary ADM models, though they were mainly focused on the neutrino fluxes induced from other operators. In addition, the studies mentioned above only focused on a few specific decay channels, while we carry out a comprehensive study of ADM decay through various operators.

The goal of this paper is two-fold. First, we aim to study the constraints from photons in the galactic center and diffuse extra galactic background on the scale M in Eq. (4) from fermionic ADM, assuming the fermionic ADM composes all (or most of) the DM. We do this both for ADM in its natural mass window (from a few GeV up to approximately 20 GeV),

and for ADM with a heavier mass near the weak scale. Second, we study models of ADM that may generate part or all of the charged cosmic ray signals observed by PAMELA, AMS-02 and H.E.S.S., consistent with the flux of anti-protons in the Universe.

There are many ADM models where the DM mass is much heavier than a few GeV. In this case a mechanism must be present to reduce the DM number density relative to the baryon number density. This can be achieved, for example, by inducing DM/anti-DM oscillations that wash out the asymmetry so that subsequent annihilations can reduce the DM number density. In this case the DM is not asymmetric from an indirect detection point of view. It is not difficult, however, to build a model where the DM is electroweak scale while retaining its asymmetry throughout the history of the Universe. One straightforward way to achieve this is to assume a non-zero primordial baryon/lepton (B/L) number in a parent particle (such as the state integrated out to generate the operators Eq. (1)) which subsequently decays with different branching fractions to the DM and the visible sectors. Such a scenario is discussed in [42–44]. As long as the DM and SM sectors are never in thermal equilibrium after decay of the heavy particles, the DM mass can be tuned to any value by changing the primordial asymmetry. In addition, the asymmetry can be diluted later in the Universe through a DM-number violating process (such as annihilation) which washes out the asymmetry; we present such a model in Appendix A.

The outline of this paper is as follows. We first discuss the details of the operators we study and specify the flavor structure for each operator in Sec. II. Then, in Sec. III, we provide details of the gamma ray flux calculation, for both the galactic and diffuse extra-galactic gamma rays. In Sec. IV we focus in detail on charged cosmic ray fluxes, both electron/positron and proton/anti-proton fluxes. In V, we discuss the results for light and heavy ADM scenarios. For heavy ADM, we find the best-fit region for electron/positron fluxes. Gamma ray spectra and proton/anti-proton fluxes are used to constrain the parameter space for both light and heavy ADM scenarios. Finally we conclude, reviewing our results.

II. OPERATORS FOR ASYMMETRIC DARK MATTER DECAY

There are many signatures that can arise from DM decay through the operators in Eq. (4). It is the purpose of this section to motivate the particular choices of flavor structures in these operators that we study below. We do not consider the $X\ell H$ operator, which is marginal and will lead to rapid DM decay.

As discussed in the introduction, in most ADM models, the mass of the DM particle is naturally $1 \sim 20$ GeV. The DM may, however, be heavier. Besides the possibility of a primordial asymmetry in the heavy particles which induce the asymmetry in DM/SM sectors through decay [42–44], we provide an alternative option in Appendix A. There we build a toy model of thermal ADM where the DM is heavier, which occurs if some X -violating interaction (mediating annihilations) is in thermal equilibrium when the temperature $T \sim m_X$. In this case, the DM number density is suppressed by a Boltzmann factor $e^{-m_X/T_{fo}}$, where T_{fo} is the temperature at which freeze-out of the X -violating interactions occurs. Since we focus on the phenomenology of ADM decay, we treat the DM mass as a free parameter, and we divide our discussion into two parts. We will first focus on the natural mass range of ADM models, i.e. $3 \text{ GeV} < m_{DM} < 20 \text{ GeV}$. Then we study the case that $100 \text{ GeV} \lesssim m_X \lesssim 10 \text{ TeV}$. We emphasize that this latter case, while motivated by models of ADM, may arise in many GUT-inspired models, such as those explored in [34, 35, 45].

In ADM models, the DM effectively carries non-zero baryon or lepton number, which may be positive or negative in sign. The gamma ray spectra are indifferent to the sign of the baryon or lepton number of the DM, but it is crucial for the charged cosmic ray measurements. We will consider both cases in our study.

The flavor structure of each model, on the other hand, is important for gamma ray observations. The possible flavor structures are many fold, and, because of the high scale of the operator, unrestricted by flavor constraints. For leptons in the final state, the electron/positron gives a hard spectrum since photons are from FSR, while the photon spectrum from tau decay is softer because of the multi-step nature of tau decay. Further, the injection spectra of the electron/positron can directly affect both electron/positron fluxes on the Earth and the gamma

ray flux from Inverse Compton (IC) processes. Thus the flavor structure in the lepton sector has large effects on observations. For operators with colored particles in the final states, the third generation is special in a two-fold manner. First, its large mass can affect the kinematic distributions of final state particles. In the low mass region, *i.e.* $3 \text{ GeV} < m_{DM} < 20 \text{ GeV}$, the b -quark mass is important for kinematics, while in the high mass region, *i.e.* $100 \text{ GeV} \lesssim m_X \lesssim 10 \text{ TeV}$, the top quark mass is important when the DM mass is a few hundred GeV. Second, the third generation quarks have different hadronization and decay products compared to the first two generations. For example, the top quark decay can contribute hard leptons in the final state.

For a light ADM mass, we treat most of the operators as flavor universal. As an example to explicitly show how flavor affects the observations, we take the \mathcal{O}_{UDD} operator and specify its decay products in two scenarios, *i.e.* light quarks only (\mathcal{O}_{UDDL}) and the heaviest quarks kinematically accessible only (\mathcal{O}_{UDDH}). As we discussed previously, however, flavor is more important for the heavy ADM scenario since electron/positron fluxes are involved. Thus for heavy ADM we study all operators in the two extremal limits, *i.e.* the lightest generation or the heaviest flavor kinematically accessible. One consequence of this flavor choice is that the decay through \mathcal{O}_{LLE} is flavor symmetric, since, due to charge conservation, there must be two oppositely charged leptons in the final states. However, if the charged leptons in the final states are not in the same generation, the asymmetric nature of the decay may become phenomenologically apparent. As an example, to highlight this unique feature of ADM models, we study one more decay channel for \mathcal{O}_{LLE} , $DM \rightarrow e^\pm + \tau^\mp + \nu(\bar{\nu})$.

In addition to the flavor structure of operators, each class of operators has several variations. As mentioned above, the Lorentz structure of the four Fermi interaction is not important for the indirect detection signals, so that we focus on the contraction integrating out the scalar particle which generates the four Fermi interaction in Eq. (4). Further, one can change the operators by taking charge conjugation on part of the operator. For example, with a small change of the field content to preserve gauge symmetry, O_{QLD} we may have not only $\frac{Xq_i l_j d_k^c}{M_{ijk}^2}$, but also $\frac{Xl_i q_j^\dagger u_k^{c\dagger}}{M_{ijk}^2}$. However, such changes leave the indirect detection signals essentially unchanged, so that we do

not study this variation of the operators further.⁴

Finally, one can also change the $SU(2)_W$ field content of the operator. For example, O_{QLD} can be changed to $\frac{Xd_i^c e_j^{c\dagger} u_k^{c\dagger}}{M_{ijk}^2}$. The new operator eliminates the hard neutrino, and only a charged lepton appears in the final state. This change impacts both the gamma ray flux and the electron/positron flux. We will take this operator as an example to illustrate the differences induced by this modification.

We summarize the combinations of operators we consider in Table I.

III. PHOTONS FROM DARK MATTER DECAY

Photons can be produced in many ways in DM decay processes. Charged particles in the final state can produce photons through bremsstrahlung. If there are colored particles in the final states, hadronization produces π^0 s, which will decay to photons. Since these photons are produced directly from the primary decay process, they are generically energetic. We will call photons from either bremsstrahlung or hadronic decays FSR γ . The other important source of photons is Inverse-Compton (IC) scattering between energetic electrons/positrons and galactic ambient light, which is mainly CMB photons and starlight. Since the galactic ambient light has very low energy, these IC photons are generically much softer than FSR photons.

In this section, for completeness, we overview the gamma ray spectra from these sources. We first focus on the gamma ray spectrum from the DM halo in our galaxy, then we will discuss the diffuse gamma ray background. We summarize the data and statistical procedure we used in our analysis.

⁴ Since the d-quark is replaced by a u-quark, the FSR spectrum may change by a small amount due to the different charges of u and d quarks. However, this change is negligible since the dominant photons are from hadronization.

Operator	light ADM	heavy ADM
lle^c	flavor universal	$e^+ + e^- + \nu$ or $\nu + \nu + \bar{\nu}$ $\tau^+ + \tau^- + \nu$ or $\nu + \nu + \bar{\nu}$ $e^+ + \tau^- + \nu$ or $\nu + \nu + \bar{\nu}$
qld^c	flavor universal	$e^- + u + \bar{d}$ or $\nu + d + \bar{d}$ $\tau^- + t + \bar{d}$ or $\nu + b + \bar{b}$
$d^c u^{c\dagger} e^{c\dagger}$	similar to qld^c not discussed	$e^- + u + \bar{d}$ $\tau^- + t + \bar{d}$
$u^c d^c d^c$	$u + d + s$ $c + b + s$	$u + d + s$ $t + b + s$

TABLE I: ADM decay operators and the flavor structures of their decays, for lle^c , qld^c , $d^c u^{c\dagger} e^{c\dagger}$ and $u^c d^c d^c$. For light ADM decay, we choose flavor universal decay for \mathcal{O}_{LLE} and \mathcal{O}_{QLD} , while for \mathcal{O}_{UDD} we choose two extremal limits as an illustration. For the gamma ray flux, \mathcal{O}_{UDE} and \mathcal{O}_{QLD} are very similar, so that we will not study \mathcal{O}_{UDE} in the low mass scenario. For heavy ADM decay, the flavor structure is important for the charged cosmic ray study. We divide our study into two extremal limits (decay to lightest generation only, and decay to heavy generation), with an additional flavor asymmetric choice for \mathcal{O}_{LLE} , which highlights the capabilities of indirect detection to tag ADM signatures. In the table, we do not distinguish the flavor of neutrinos, and we present only the decay products for ADM carrying positive B or L number, though we consider ADM with both positive and negative B(L) number in our study.

A. Photon Flux from DM Decay

1. Galactic DM Halo

The galactic DM halo provides a promising place to look for the gamma ray flux produced through DM decay processes, where the FERMI collaboration has released the sky map of the gamma ray measurement up to a few hundred GeV [46, 47]. Electrons/positrons propagating

in the galaxy scatter with starlight, as well as infrared and CMB photons to produce Inverse-Compton photon. The spectrum from IC scattering, especially in the inner galaxy, depends strongly on details of the galaxy, such as starlight spectrum and distribution. To avoid introducing large uncertainties, we do not consider the IC spectrum and only focus on the FSR γ for the galactic halo constraints.

The flux of photons from DM decay in our galaxy can be written as

$$\frac{dJ_\gamma}{dEd\Omega} = \frac{1}{4\pi\tau_{DM}m_{DM}} \frac{dN_\gamma}{dE} \int_{l.o.s.} ds \rho_{DM}(r) \quad (7)$$

where the integral is along the line of sight, $\frac{dN_\gamma}{dE}$ is the gamma ray spectrum from ADM decay, and $\rho_{DM}(r)$ is the DM profile in our galaxy. We choose an *NFW* profile,

$$\rho_{DM}(r) = \rho_s \left(\frac{r_s}{r}\right) \left(1 + \frac{r}{r_s}\right)^{-2} \quad (8)$$

with $r_s = 24.42$ kpc and $\rho_s = 0.184$ GeV/cm³. To get the gamma ray spectrum from DM decay, i.e. $\frac{dN_\gamma}{dE}$, we use MadGraph to generate parton level events, and use PYTHIA to shower and hadronize the events.

2. Extra-galactic γ -ray

In addition to the galactic halo, the gamma ray flux from the decay or annihilation of DM particles in the early Universe can propagate to the Earth and contribute as a diffuse extra-galactic gamma ray background. The measurement of the diffuse extra-galactic gamma ray spectrum is provided by FERMI in [48], and provides a particularly important constraint on DM decay. The ratio of extra-galactic gamma ray flux from DM decay, $\Phi_{exG-\gamma}$, to the galactic halo gamma ray flux, Φ_{halo} , can be estimated as,

$$\frac{\Phi_{exG-\gamma}}{\Phi_{halo}} \sim \frac{\rho_{cosmo} R_{cosmo}}{\rho_\odot R_\odot} \sim 1, \quad (9)$$

where ρ_{cosmo} is the average DM energy density in the Universe, R_{cosmo} is the size of the Universe, ρ_\odot is the local DM energy density and R_\odot is the distance from the solar system to the galactic

center. Due to this numerical coincidence, the constraints from the diffuse extra-galactic gamma ray flux are comparable to the constraints from the galactic halo.

There are again two dominant contributions to extra-galactic gamma rays, one from FSR γ and the other from scattering between hard electron/positrons produced from the decay and the soft photon background. Unlike in the galaxy, the IC scattering is dominated by scattering off CMB photons. Since the uncertainty is rather small in this case, we will include the IC contribution to the diffuse extra-galactic gamma ray flux.

For the photons produced directly from DM decay, the spectrum can be calculated by properly redshifting the photon injection spectrum at any redshift z . High energy photons can be absorbed in a cosmological length. The dominant absorption is caused by the scattering with CMB photons. This is only important, however, for extremely high energy photons. For the energy range we consider in this paper, *i.e.* E_γ smaller than few TeV , the absorption is negligible. Given an injection spectrum from DM decays at redshift $a = 1/(1+z)$, *i.e.* $\frac{dN_{\gamma,FSR}}{dE_\gamma(a)}$, the flux of photons is

$$\frac{d^2\Phi_{\gamma,EG,FSR}}{d\Omega dE_\gamma} = \frac{c \Omega_{DM} \rho_c}{4\pi\tau M_{DM}} \int_0^1 \frac{da}{a^2} \frac{1}{H_0 \sqrt{\Omega_\Lambda + \Omega_m/a^3}} \frac{dN_{\gamma,FSR}}{dE_\gamma(a)}. \quad (10)$$

We take $\Omega_m + \Omega_\Lambda \simeq 1$ and $\Omega_{DM} \rho_c \simeq 1.3 \times 10^{-6} \text{GeV}/\text{cm}^3$, when calculating the gamma ray flux from prompt photons.

To estimate the gamma ray flux from the IC scattering between high energy electrons/positrons and CMB photons, we closely follow the procedure of [49]. For low energy photons in the CMB, the radiation power and the energy loss coefficient function are computed in the Thomson limit. This simplifies the calculation. Further, the mean free path of the electron/positron in the intergalactic medium is much shorter than the cosmological length, so that one can approximately treat the IC spectrum as injected instantaneously, $\frac{dN_{\gamma,IC}}{dE_\gamma(a)}$. Similar to Eq. (10), by properly redshifting the IC spectrum, one obtains the IC contribution to the extra-galactic gamma ray.

When the DM mass is small, the IC contribution to the extra-galactic gamma spectrum is negligible. However, when the DM is very heavy, *e.g.* $O(\text{TeV})$, the IC contribution is dominant. We will see this explicitly when we discuss the heavy ADM scenario.

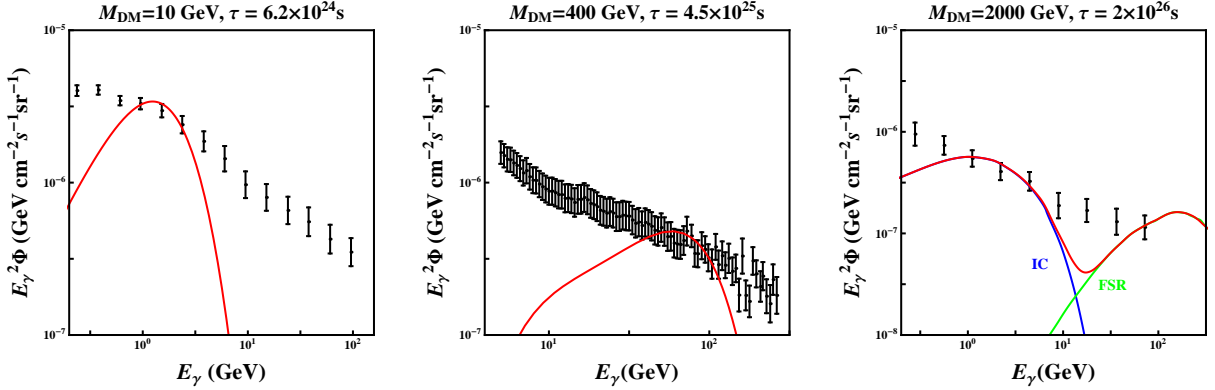


FIG. 1: From left to right, we show the Fermi galactic low energy data [46], the Fermi galaxy high energy data [47], and the Fermi diffuse extragalactic gamma ray data [48]. We also show the ADM decay spectra through the \mathcal{O}_{LLE} operator assuming a flavor universal structure, shown as red curves. For the extragalactic gamma ray flux, when the DM mass is large, both FSR and IC contributions are important. The decay lifetime is chosen so that gamma ray from DM decay does not exceed any bin by $1 - \sigma$.

B. Data and Statistical Methodology

For the galactic gamma ray spectrum, the FERMI collaboration provides two sets of measurements which we use. One is focused on the low energy regime, ranging from 0.2 GeV to 100 GeV [46]. In this measurement, the gamma ray spectrum is provided on different patches on the sky. We choose the patch of the full sky without the galactic plane, i.e. $0^\circ \leq l \leq 180^\circ$ and $8^\circ \leq b \leq 90^\circ$. When the DM mass is small, the low energy measurement is the most sensitive probe. The other measurement from the FERMI collaboration is in the high energy regime, from 4.8 GeV to 264 GeV [47]. The region of coverage is the full sky minus the galactic plane while keeping galaxy center, i.e. $(|b| > 10^\circ)|(l \leq 10^\circ)|(l \geq 350^\circ)$. This will be more useful for constraining the heavy ADM decay scenario. For the diffuse extra-galactic gamma ray spectrum, we take the most recent published measurement from FERMI [48]. In Fig. 1, we overlay all the data sets we use for our gamma ray analysis.

In this paper we provide the most conservative constraints on the ADM decay scenario from gamma ray spectra. We require the flux from ADM decay does not exceed the central value plus twice the error bar in any bin, without any assumption about the background flux. One could improve the constraints by subtracting the astrophysical background, gaining perhaps a factor of a few on the constraints. This, however, induces larger systematic uncertainties from the background. For this reason, we focus on the most conservative analysis.

IV. CHARGED PARTICLES FROM DARK MATTER DECAY

In this section, we focus on charged particle fluxes induced by DM decay. As noted in the introduction, unlike in previous studies, the ADM operators we employ, *i.e.* Eq. (1), both generate the DM asymmetry and induce DM decay, so that in this case the cosmic ray signals are a signature for the ADM mechanism itself. At minimum, the asymmetry of the DM impacts signatures through the sign of the baryon or lepton number that the DM carries, which in turn determines the nature of the decay products. Since the signatures depend on the B/L sign, we will consider both cases. In addition, as usual, the flavor structure of the operators affects the signatures substantially, especially for the study of best-fit region for electron/positron fluxes, as summarized in Table I. For the light DM scenario, we study the flavor universal scenario except for \mathcal{O}_{UDD} . For the heavy DM scenario, we will take two extremal cases in this section – DM decaying to the first generation only, or to the third generation only; other flavor combinations fall between these two choices. In addition, for the \mathcal{O}_{LLE} operator we make another flavor choice, decay to $e^+\tau^-\nu$, that highlights the asymmetric nature of the decay. When DM is a symmetric relic, generically, one expects the same spectra of electrons and positrons in the final state.⁵ However, this is not necessarily the case for ADM – since there may be no hard electrons in the final state, the positron ratio from DM decay alone can be as high as 1, and

⁵ There are some special cases where even symmetric dark matter decay can induce asymmetric electron/positron spectra. One example is assuming DM is a Majorana fermion with several different decay channels. If there is a non-trivial CP-violating phase, then the electron/positron spectra in the final states can be different from each other. This scenario is realized in [16], though not aimed at inducing DM decay.

since there are no hard electrons in the final state, the number of hard photons from FSR as well as IC is reduced. These special features of the ADM scenario help to reduce the tensions between the AMS-02 anomaly and other measurements [40].

We have already discussed in Sec. III the methods that we use for constraining ADM decay with photons. Thus in this section, we will focus on the electron/positron flux and proton/anti-proton flux, where we provide details on the data we use and the statistics we apply. In Sec. V, we present our results by combining all channels for indirect detection, both gamma and charged cosmic rays.

1. e^+/e^- Fit from AMS-02 and H.E.S.S.

In 2008, PAMELA [50] published their measurements of the electron/positron fluxes, showing that the positron fraction rises at energies above few GeV. Recently AMS-02 [51] confirmed PAMELA's result but with smaller uncertainties and extending to higher energies. Since ADM decays to quarks and leptons through the operators in Eq. (1), it is interesting to see how well the electron/positron flux can be fitted by these operators. We use AMS-02 data only for our fit in low energy regime; since AMS-02 is in good agreement with PAMELA, we do not expect inclusion of the PAMELA data to substantially change our result. This reduces the uncertainties on combining different data sets from different experiments. For the total e^\pm flux measurement, we fit the AMS-02 and H.E.S.S. data (the latter being relevant only at the highest energies). We do not include Fermi. The measurements of Fermi and AMS-02 disagree below 100 GeV so that including both Fermi and AMS-02 data would give rise to a poor fit. We have checked that including Fermi instead of AMS-02 data in our fits does not substantially change our result, since in that case the fit simply prefers a different astrophysical background. Further work and measurement will be required to resolve the systematic difference between Fermi and AMS-02 below 100 GeV.

To obtain the electron/positron fluxes received near the Earth, we use GALPROP to calculate the propagation [54]. We run the 2D mode of the code, which calculates the propagation equations on (r, z) grid. We use the same DM distribution profile applied in previous studies,

i.e. Eq. (8), and we choose the propagation parameters in a conventional way. The diffusion constant $K(E)$ is taken to be $5.8 \times 10^{28} (E/4 \text{ GeV})^{0.33} \text{ cm}^2/\text{s}$, and the root-mean-square of the magnetic field is modeled by an exponential disk,

$$B_{\text{rms}} = B_0 \exp(-(r - R_{\odot})/r_B - |z|/z_B) \quad (11)$$

where $B_0 = 5 \mu\text{G}$, $r_B = 10 \text{ kpc}$ and $z_B = 2 \text{ kpc}$.

To estimate how well electron/positron fluxes constrain the decay lifetime, we carry out a χ^2 fit including an astrophysical background, which we take to be [55, 56]

$$\begin{aligned} \Phi_{e^-}^{(prim)}(E) &= \frac{0.16e^{-1.1}}{1 + 11e^{0.9} + 3.2e^{2.15}} (\text{GeV}^{-1} \text{cm}^{-2} \text{s}^{-1} \text{sr}^{-1}) \\ \Phi_{e^-}^{(sec)}(E) &= \frac{0.7e^{0.7}}{1 + 110e^{1.5} + 600e^{2.9} + 580e^{4.2}} (\text{GeV}^{-1} \text{cm}^{-2} \text{s}^{-1} \text{sr}^{-1}) \\ \Phi_{e^+}^{(sec)}(E) &= \frac{4.5e^{0.7}}{1 + 650e^{2.3} + 1500e^{4.2}} (\text{GeV}^{-1} \text{cm}^{-2} \text{s}^{-1} \text{sr}^{-1}) \end{aligned} \quad (12)$$

where $e = \frac{E}{1 \text{ GeV}}$. To treat the background uncertainties, we allow variation in both overall normalization and index of the power law. More precisely, we take

$$\begin{aligned} \Phi_{e^-}(E) &= A_- e^{P_-} (\Phi_{e^-}^{(prim)}(E) + \Phi_{e^-}^{(sec)}(E)) \\ \Phi_{e^+}(E) &= A_+ e^{P_+} \Phi_{e^+}^{(sec)}(E) \end{aligned} \quad (13)$$

where $0 < A_{\pm} < +\infty$ and $-0.05 < P_{\pm} < 0.05$. To fit the AMS-02/H.E.S.S. data, we took both the positron ratio and e^{\pm} total flux with 6 parameters, A_{\pm} , P_{\pm} , m_{DM} and τ . We only take the bins with energy larger than 10 GeV in order to reduce the uncertainties from solar modulation. Further, to fit the total electron/positron flux from H.E.S.S. measurement, we include the 15% systematic uncertainty in the energy calibration as following:

$$\chi_{H.E.S.S.}^2 = \min \left\{ \sum_i \frac{(\Phi_i^{DM}(E_i(1+e)) - \Phi_i^{exp})^2}{\delta\Phi^2} + \frac{e^2}{\delta e^2} \mid e \right\} \quad (14)$$

where the sum runs over all bins in H.E.S.S. data, and we take δe as 15%. Later, we present the 3-sigma best fit region in the $(m_{DM} - \tau)$ plane.

To illustrate how well one can fit AMS-02 and H.E.S.S. data, we choose several benchmark points and show the comparison between the fit and the data. For positron ratios, we extend curves beyond current energy range to show how various models behave as more AMS-02 data is accumulated. Complete results for different ADM operators will be shown below, in Sec. V.

2. Constraints from p^+/p^- Fluxes

For operators we are considering, DM decay products may include quarks so that modifications of the proton/anti-proton fluxes are possible. The best data for the proton flux is from AMS-02 [57], while PAMELA provides the most updated results for the anti-proton flux and anti-proton/proton ratio [58, 59]. For proton/anti-proton fluxes, the data agrees well with the astrophysical expectation, so that we use this data to constrain the decay lifetime for each operator. Unlike the electron/positron fluxes, the anti-proton flux is much smaller than the proton flux, with the ratio being $\sim 10^{-4}$ in the energy range of interest. Proton and anti-proton fluxes are dominantly from the hadronization of colored particles in the DM decay final states, with the flux of protons comparable to anti-protons. Thus after adding in the contribution of DM decay, the anti-proton flux can be changed significantly while the proton flux remains almost unchanged, implying that the constraint from anti-proton ratio should be much stronger than that from proton/anti-proton total flux.

To compute the anti-proton flux as a constraint on ADM decay, we applied GALPROP to calculate the propagation of the proton/anti-proton flux, where the parameters are the same as in Sec. IV 1. The solar modulation effect is important in low energy bins. For the heavy ADM scenario, to reduce the uncertainties in the solar modulation calculation of the fluxes, we focus on proton/anti-proton fluxes whose kinetic energy is larger than 1 GeV. On the other hand, the data in the low energy region is important for the light ADM scenario. To properly estimate the constraint on the decay lifetime, we use a force-field approximation to model the solar modulation:

$$J(E) = \frac{E^2 - m^2}{(E + \phi)^2 - m^2} J_{IS}(E + \phi) \quad (15)$$

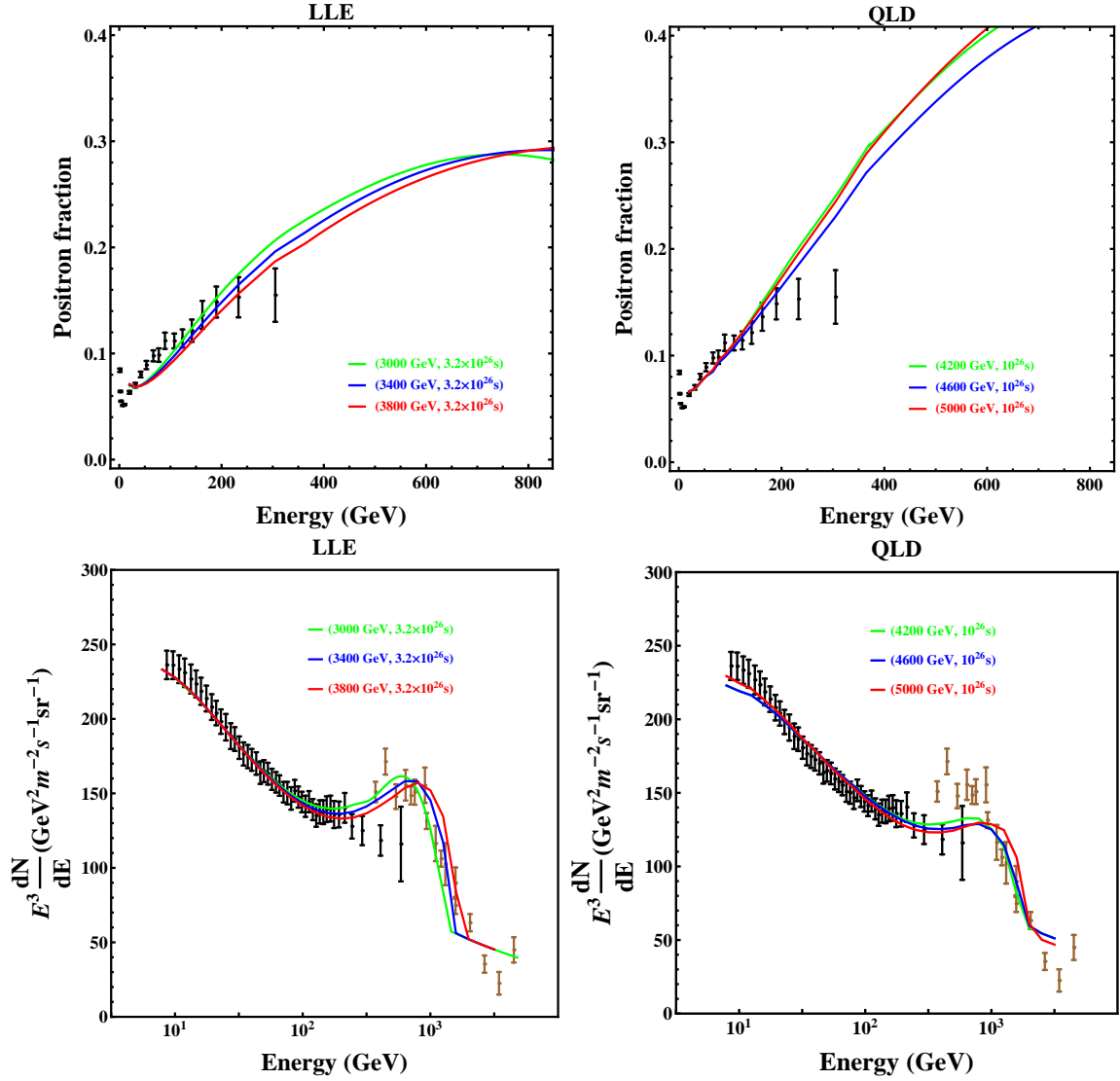


FIG. 2: Benchmark points of the electron/positron spectra. *Left*: DM decay through the \mathcal{O}_{LLE} operator, with first generation fermions in the final states only. DM masses are taken to be 3 TeV, 3.4 TeV and 3.8 TeV, with the decay lifetime fixed at 3.2×10^{26} s. *Right*: DM decay through \mathcal{O}_{QLD} , with first generation fermions in the final states only. DM masses are taken to be 4.2 TeV, 4.6 TeV and 5 TeV, with decay lifetimes fixed at 10^{26} s. Data points are taken from the recent AMS-02 results [51] and H.E.S.S. measurements [52, 53]. For positron ratios, we extend curves beyond the current energy range, to show how AMS-02 data might appear at higher energies.

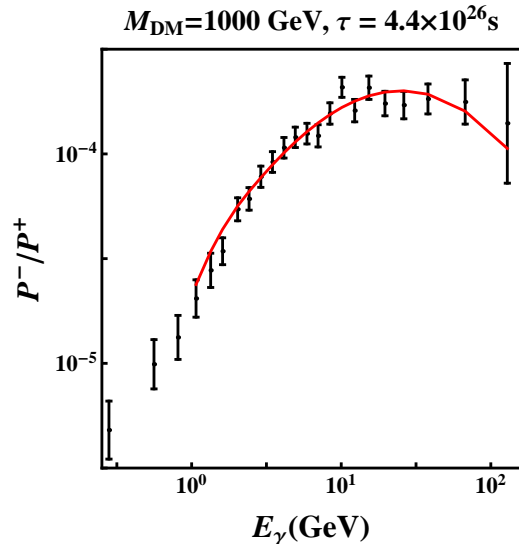


FIG. 3: Anti-proton to proton flux ratio for a benchmark ADM decay, adding the DM proton/anti-proton fluxes to the astrophysical background, and comparing with PAMELA data [58]. The DM mass is 1 TeV, the decay operator \mathcal{O}_{QLD} with only first generation particles in the final states, and a lifetime 4.4×10^{26} s.

where E is the total energy of the proton, m is proton mass. J_{IS} is the interstellar cosmic ray flux before accounting for the effect of solar modulation, and $J(E)$ is the cosmic ray flux after correcting solar modulation effects. ϕ is the modulation parameter which is taken to be 500 MeV.

To model the astrophysical background of proton and anti-proton fluxes, we fit the proton/anti-proton fluxes as sum of polynomials. Similar to the electron/positron cases, we allow small variations in both the overall normalization and the index of the power law, $0 < A_{\pm} < +\infty$ and $-0.05 < P_{\pm} < 0.05$. For each DM mass, we find the values of A_{\pm} , P_{\pm} and τ which best fit the data. Then we constrain the DM decay lifetime at the 2σ level with respect to the best fit point. We show a benchmark \mathcal{O}_{QLD} model point which is constrained at the 2σ level in Fig. 3.

V. CONSTRAINTS ON ADM DECAY

A. Light ADM Scenario

We begin with constraints on ADM particles with mass in the natural window, around 10 GeV. We take the flavor universal scenario for both \mathcal{O}_{LLE} and \mathcal{O}_{QLD} operators, while for \mathcal{O}_{UDD} , we take both the heavy and light flavor structure, \mathcal{O}_{UDDL} and \mathcal{O}_{UDDH} , as discussed in Table I. This choice aims to illustrate the effects of final state quark kinematics including the b -quark threshold effect.

As discussed in previous sections, we derive constraints on light ADM decay by gamma ray spectrum and proton/anti-proton fluxes. In Fig. 4, we present our results. For each operator, we overlay the constraints from gamma ray spectra with those from proton/anti-proton fluxes.

For the constraints from gamma ray spectra, the constraints are stronger when there are more hadronic particles in the final state, as expected. The constraints on \mathcal{O}_{UDDL} are universally stronger than the constraints on \mathcal{O}_{UDDH} , since quarks from \mathcal{O}_{UDDL} have larger kinetic energy.

For proton/anti-proton fluxes, the constraints are very different when DM carries positive or negative baryon number. When DM carries negative baryon number, there is at least one anti-proton in the decay final states. As illustrated in Fig. 2, the anti-proton fraction is about $10^{-5} \sim 10^{-4}$. This is sensitive to the number of anti-protons injected by DM decay, which gives a much stronger constraint on decay lifetime when DM carries negative baryon number. On the other hand, the lepton number carried by DM particles does not make a difference for $p + /p-$ fluxes. Thus the constraints for \mathcal{O}_{QLD} from $p + /p-$ are the same.

There are discontinuities in the constraints of \mathcal{O}_{UDDH} , both for gamma ray spectra and $p + /p-$ fluxes. The discontinuities show up at around 7 GeV. This is caused by the change of final state kinematics due to the open of b -quark decay channel.

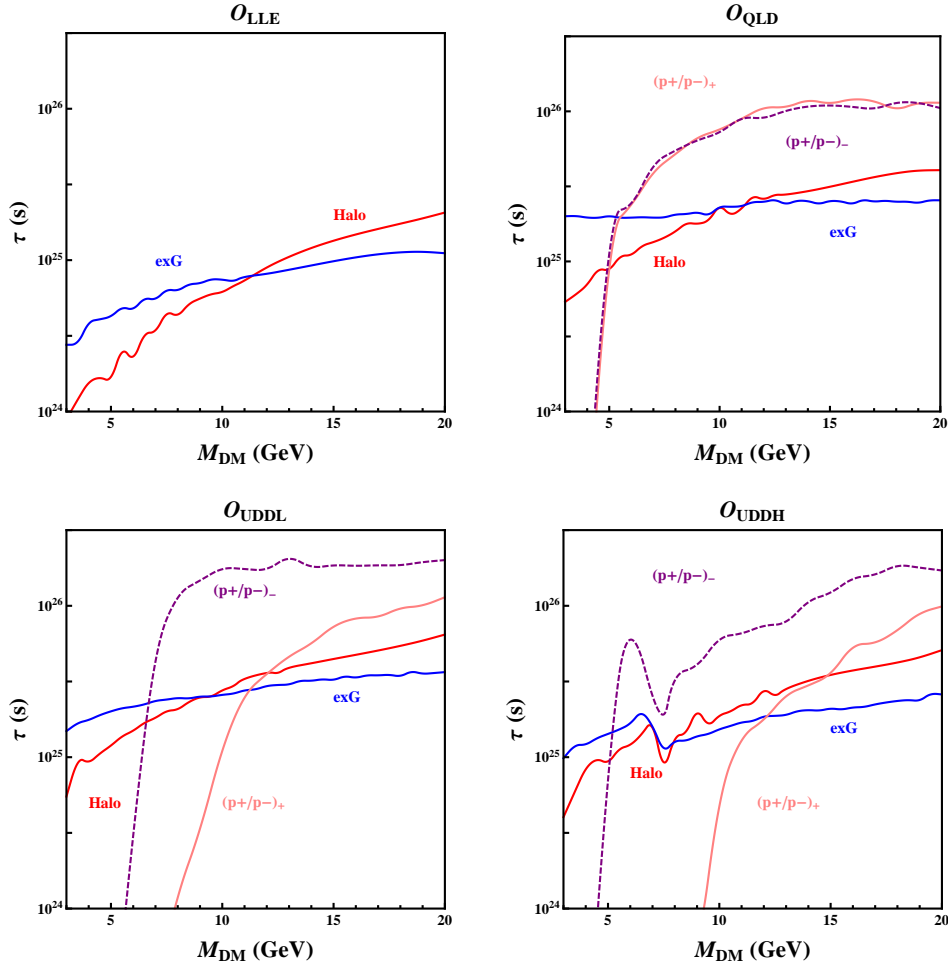


FIG. 4: Constraints on the lifetime τ of the DM from gamma ray spectra and from proton/anti-proton fluxes. We consider both scenarios where the ADM particle carries positive or negative baryon/lepton number. As expected, the sign of baryon number is important for the constraints from $p + /p-$.

B. Heavy ADM scenario

The goal of this section is to show both how gamma- and charged cosmic rays constrain heavy ADM (with mass between 100 GeV and 10 TeV), and how heavy ADM decay may generate the rising feature of the positron-to-electron ratio observed in PAMELA and AMS-02.

In the previous sections, we addressed each indirect detection channel carefully. Now we

combine all channels for each operator to examine in detail whether there are regimes in parameter space which can fit AMS-02 while remaining consistent with other constraints. For the two extremal flavor choices, *i.e.* lightest and heaviest generation fermions in the final states, the combined results are shown in Figs. 5, 6. For the flavor asymmetric decay of \mathcal{O}_{LLE} , *i.e.* $DM \rightarrow e^\pm + \tau^\mp + \nu(\bar{\nu})$, the combination of various channels is presented in Fig. 7.

As we discussed previously, ADM can carry either positive or negative B/L number. Obviously this does not affect the gamma ray spectrum, but it is crucial for studies of charged cosmic rays as can clearly be seen in Figs. 5-7. The difference is obvious for \mathcal{O}_{QLD} and \mathcal{O}_{UDE} operators, as well as for the flavor asymmetric decay of \mathcal{O}_{LLE} , though when the decay products involve the lightest generation, the difference is maximally enhanced on account of the hard lepton in the final state. If \mathcal{O}_{QLD} or \mathcal{O}_{UDE} carries negative lepton number, then the hard lepton is a positron, and similarly for the asymmetric decay of \mathcal{O}_{LLE} . Since the rising feature in the positron fraction is most sensitive to the hard positron in the final states, this substantially affects the fits.

From Figs. 5-7, we see the best fit regions are confined to be small ellipses. The positron data prefers fairly heavy DM, with mass above several hundred GeV, and since the current data for the positron ratio stops around 300 GeV, it does not impose an upper limit on the DM mass. On the other hand, the electron/positron total fluxes provide further constraints on both the very low and very high DM mass region. In particular, data from the H.E.S.S. measurement does not connect to the AMS-02 data smoothly. A bump appears around 1 TeV when we combine these two data sets, which imposes a preference for a DM mass around a few TeV, as illustrated in Fig. 2.

In the ADM decay scenario, one may have hard positrons in the final states without generating an equal number of electrons. This helps to reduce the energetic byproducts from the decay, including the gamma ray flux associated with the charged leptons. Unfortunately, when we combine our results from the electron/positron ratio with other constraints, the preferred region is still in tension with other measurements, especially the diffuse extra-galactic gamma ray flux. This is largely because the H.E.S.S. feature around 1 TeV imposes a lower bound

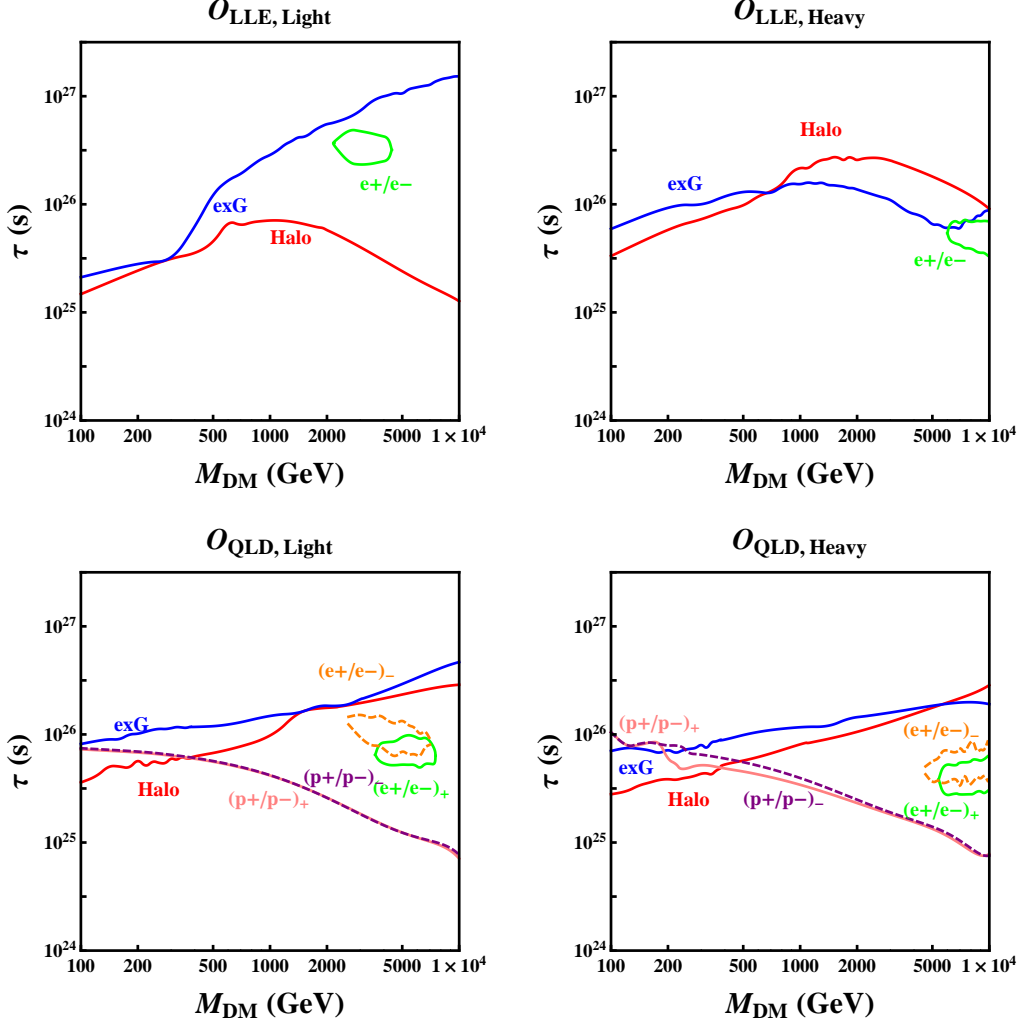


FIG. 5: Combination of constraints and best fit regions for \mathcal{O}_{LLE} and \mathcal{O}_{QLD} operators. As discussed in the text, constraints (*i.e.* the lower limits on DM decay lifetime) are placed at $2\text{-}\sigma$ level, while the best fit ellipses for AMS-02 and H.E.S.S. electron/positron data are shown at $3\text{-}\sigma$. The left panels assume the decay products prefer the lightest generation, while the right panels assume the heaviest generation kinematically available is favored. We overlay the results for ADM with positive/negative B(L) number for charged cosmic ray fluxes, while the gamma ray constraints are the same for these two cases. The solid lines of charged cosmic rays are for positive B(L) number and the dashed lines are for negative B(L) number.

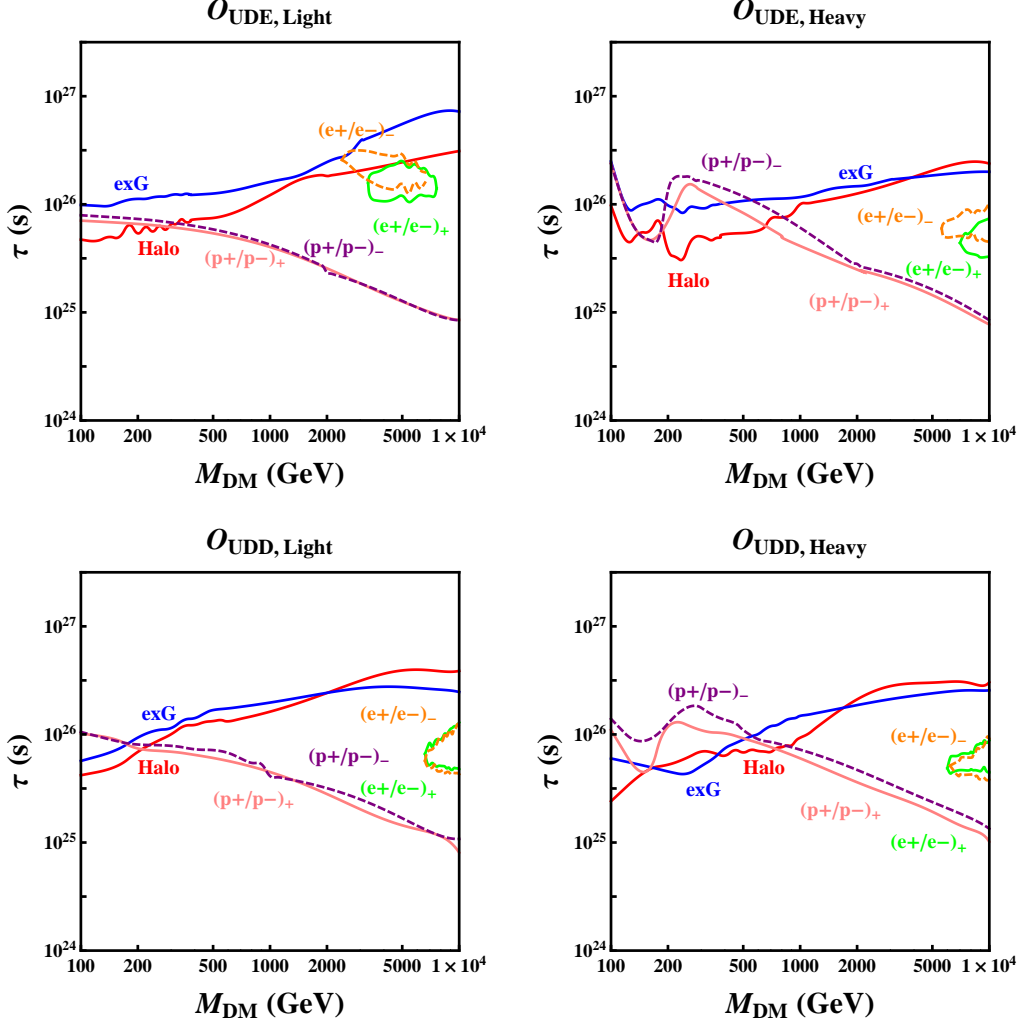


FIG. 6: Combination of constraints and best fit regions for \mathcal{O}_{UDE} and \mathcal{O}_{UDD} operators. As discussed in the text, constraints (*i.e.* the lower limits on DM decay lifetime) are placed at $2\text{-}\sigma$ level, while the best fit ellipses for AMS-02 and H.E.S.S. electron/positron data are shown at $3\text{-}\sigma$. The left panels assume the decay products prefer the lightest generation, while the right panels assume the heaviest generation kinematically available is favored. We overlay the results for ADM with positive/negative B(L) number for charged cosmic ray fluxes, while the gamma ray constraints are the same for these two cases. The solid lines of charged cosmic rays are for positive B(L) number and the dashed lines are for negative B(L) number.

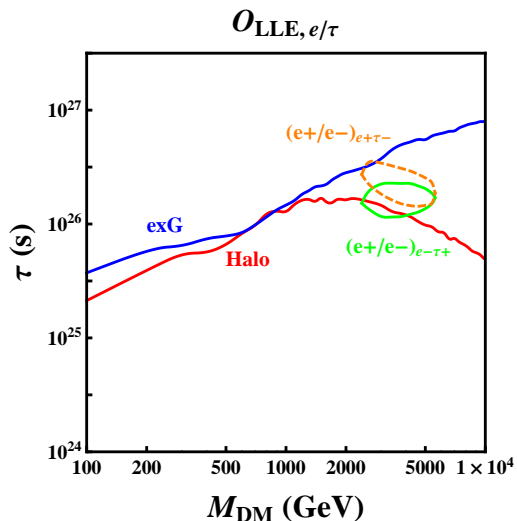


FIG. 7: Combination of constraints and best fit regions for \mathcal{O}_{LLE} operator with the flavor asymmetric decay $X \rightarrow e^\pm + \tau^\mp + \nu(\bar{\nu})$. As discussed in the text, constraints are placed at $2\text{-}\sigma$ level, while the best fit of AMS-02 and H.E.S.S. electron/positron data is shown at $3\text{-}\sigma$. We overlay the results for ADM with positive/negative B(L) number for charged cosmic ray fluxes, while the gamma ray constraints are the same for these two cases. The solid line fits to AMS-02/H.E.S.S. data are for e^-/τ^+ decay while the dashed lines are for e^+/τ^- decay.

on the preferred DM mass. This feature, however, appears at the connection region between the two data sets, which is worrisome (recall that a similar type of feature appeared in the ATIC data at lower energy before both Fermi and AMS-02 concluded that no such feature was present). Having a better statistics measurement of electron/positron total flux at higher energy is thus necessary for drawing any definite conclusions from this analysis.

As noted above in Table I, and in Figs. 5-6, we chose to present two extremal limits, decay to the heaviest or lightest generation. Taking \mathcal{O}_{LLE} as an example, comparing the two extremal flavor cases, when the heaviest generation, *i.e.* τ , is preferred, the constraint from the galactic halo gamma ray flux is much stronger on account of the photons from hadronic τ decay. On the other hand, the electron/positron spectra are much harder when the first generation leptons are preferred in the decay products. This has two consequences. First, a harder IC contribution to

the diffuse extra-galactic gamma ray flux is present, which leads to a much stronger constraint when the DM mass is large. Second, since the rising feature of the positron ratio in the AMS-02 data is easier to fit, a longer decay lifetime is preferred. Although the best-fit region from the e^\pm measurement is in tension with gamma ray measurement in both scenarios, the tension is much weaker when DM only decays to first generation fermions. Similar arguments can also be applied to other operators as one can see from Figs. 5-7.

When the up-type quark is involved in the final state, whether the top quark is kinematically allowed is the most important feature.⁶ For example, for DM decaying through the \mathcal{O}_{UDE} or \mathcal{O}_{UDD} operator, as can be seen in Fig. 6, when the heaviest generation fermions are preferred, the constraint from proton/anti-proton fluxes around 200 GeV is not smoothly connected to that in higher mass region. This feature around the top quark threshold is not as pronounced for \mathcal{O}_{QLD} in Fig. 5, which is mainly because \mathcal{O}_{QLD} has two decay channels for third generation particles in the final states, *i.e.* $DM \rightarrow \tau^- + t + \bar{d}$ and $DM \rightarrow \nu + b + \bar{b}$.

To summarize, in the ADM decay scenario considered in this paper, the best fit regions from the electron/positron analysis are in tension with other measurements for all operators we consider. This is largely due to the rising feature in the H.E.S.S. data around 1 TeV, which needs to be further investigated with better measurements from AMS-02 before a definite conclusion can be drawn. For \mathcal{O}_{LLE} , \mathcal{O}_{QLD} and \mathcal{O}_{UDE} , the tension is much weaker than from \mathcal{O}_{UDD} , as expected. As is well known, the flavor structure of these operators is also crucial. If the third generation particles are dominant in the final states, the tension is much stronger. We also showed that whether ADM carries positive or negative B(L) number has impact on the signatures, providing a possible handle to probe the asymmetry generating mechanism of ADM.

⁶ A similar phenomenon also appears for the light ADM scenario when the bottom quark is involved.

VI. CONCLUSIONS

In this paper we have studied signatures for decaying ADM through a higher dimension operator. While most models of ADM in the literature have assumed that the ADM is absolutely stable (*e.g.* through a Z_2 symmetry or through R -parity), the apparent stability of the DM may simply be due to a very high suppression scale of the higher dimension operator. These same higher dimension operators, as shown in Eq. (1), are responsible for the asymmetry generation in the DM sector. Thus one may be able to connect indirect detection signatures to the ADM mechanism. In addition, the asymmetry in the DM sector gives unique signatures that allow one to prove through indirect detection the *sign* of the B/L number carried by the DM.

We focused on four Fermi interactions, where a suppression scale M for the operator just below the GUT scale is sufficient to be consistent with all constraints. We considered both ADM in its natural mass window around 10 GeV, as well as heavier ADM with mass between 100 GeV and 10 TeV. In the former case, we study the constraints from both gamma ray spectra and proton/anti-proton fluxes; generally the constrained lifetime translates to a constraint on the suppression scale of around 10^{13} GeV. For heavier ADM, we fit AMS-02 and H.E.S.S. data to the models and consider constraints from high energy FERMI data as well as the proton/anti-proton fluxes in PAMELA. In this case, a suppression scale of around $10^{15} - 10^{16}$ GeV is appropriate for fitting AMS-02 and H.E.S.S. data. We were able to demonstrate the effect of the sign of the ADM B/L asymmetry on the signatures.

Determining the nature of the DM is a complex multi-faceted problem. Further determining how the DM density is set, for example through a cosmic asymmetry, is an even greater challenge. Astrophysical objects, such as stars and neutron stars can also be crucial probes, though they give no hint as to how the asymmetry was generated in the first place in the DM sector. (See [10] and the references therein for review.) For ADM communicating with the SM through higher dimension operators, if the suppression scale of the operator is between 1 TeV and 10^4 TeV, collider and flavor signatures are relevant for probing ADM, as explored in [60]. For a much higher suppression scale, around the GUT scale, however, one may worry that determining the nature of the ADM mechanism becomes essentially impossible. Here we have

shown that indirect detection in these cases may provide a handle, lending one more tool in the hunt for the DM.

Acknowledgments

We would like to thank Marco Cirelli, Jeremy Mardon, Michele Papucci, Paolo Panci, Alessandro Strumia, Meng Su, Wei Xue for helpful discussions. The work of KZ is supported by NASA astrophysics theory grant NNX11AI17G and by NSF CAREER award PHY 1049896. YZ is supported by ERC grant BSMOXFORD no. 228169 and NSF grant PHY-1316699.

Appendix A: A Toy Model for Heavy ADM

In most ADM models, the DM particle's mass is naturally around a few GeV. Small variations in the model, however, can easily bring the DM mass out of its natural range. In this section, we provide a toy model for heavy ADM with the asymmetry generated via Eq. (1). The ADM retains its asymmetry through this process.

Given a concrete model, once DM and SM sectors are in equilibrium, the baryon number deposited into the DM sector is fixed. If there is only one component of DM, the DM mass is fixed by DM energy density Ω_{DM} . However, if there are multiple particles in the DM sector, for example if one is heavy and one is light, the light DM particles can carry more of the baryon number of the entire sector while the heavy DM particles contribute dominantly to Ω_{DM} . Such a model can be easily built, and here we present our toy model following this logic. We assume there are two components of DM particles, X and ϕ , and the Lagrangian for interactions in the DM sector is written as

$$\mathcal{L}_{DM} = \frac{y}{2} X_L X_L \phi^* - \frac{y}{2} X_R^c X_R^c \phi + h.c. + \frac{\lambda}{4} \phi^2 \phi^{*2}, \quad (\text{A1})$$

where X_L and X_R^c are two Weyl spinors components of X . X carries one unit of baryon/lepton number, depending on how X couples to SM sector. ϕ is a complex scalar field which carries two units of B/L number. We assume m_X is much larger than m_ϕ .

If we assume that the transfer of the SM baryon or lepton number to the DM sector decouples at a high temperature, the baryon or lepton number in the DM sector is locked. The details are highly model dependent, but the ratio of the primordial asymmetries in the two sectors is $\mathcal{O}(1)$.

When the temperature drops below the transfer decoupling temperature, the interaction within the DM sector is still active. Due to B conservation, there is no 2-to-2 process (if we restrict ourselves to marginal operators for the annihilation)⁷ capable of transferring baryon number from X to ϕ . One has to rely on a 2-to-3 process, *i.e.* $X + X \rightarrow 2\phi + \phi^*$. The scattering cross section for this process is

$$\sigma v \sim \frac{y^2 \lambda^2}{8192 \pi^3 m_X^2}, \quad (\text{A2})$$

which controls the abundance of X in the DM sector. We label the temperature when this 2-to-3 process freezes out as $T_{X,\phi}$. This is the freeze-out temperature of the chemical equilibrium between X and ϕ . We assume that the freeze-out temperature for kinetic equilibrium is much lower than $T_{X,\phi}$. Thus both X and ϕ are thermal, and their number densities are described by a Boltzmann distribution at $T_{X,\phi}$. This is a reasonable assumption, because one needs a large annihilation cross section to deplete the symmetric component of ADM.

If $T_{X,\phi}$ is larger than m_X , both X and ϕ are relativistic. The asymmetries of number densities in X and ϕ depend on the chemical potentials as

$$\Delta n_i = \frac{g_i T_{DM,SM}^3}{6\pi^2} \left[\pi^2 \left(\frac{\mu_i}{T_{DM,SM}} \right) + \left(\frac{\mu_i}{T_{DM,SM}} \right)^3 \right] \simeq \frac{g_i T_{DM,SM}^3}{6} \left(\frac{\mu_i}{T_{DM,SM}} \right). \quad (\text{A3})$$

Since the chemical potentials for X and ϕ only differ by a factor of 2, the asymmetries carried by these two particles are still comparable to each other. Thus the DM mass cannot be too large to obtain the correct DM density.

If instead $T_{X,\phi} < m_X$, X is non-relativistic while ϕ is relativistic. For non-relativistic

⁷ If we instead allow the annihilation to proceed through higher dimension operators (for example through an interaction $XX'\phi$, where X' is exchanged in the t -channel and is heavier than X), 2-to-2 annihilation $XX \rightarrow \phi\phi$ may proceed, though suppressed by the mass scale of the particle (X' here) being integrated out. The essential dynamics of the models we consider below is unchanged, though some numbers will be modified.

particles, the chemical potential is related to the number density difference as

$$\Delta n_i = 2g_i \left(\frac{m_i T_{X,\phi}}{2\pi}\right)^{3/2} \text{Sinh}[\mu_i/T_{X,\phi}] e^{-m_i/T_{X,\phi}} \simeq \frac{2g_i \mu_i}{T_{X,\phi}} \left(\frac{m_i T_{X,\phi}}{2\pi}\right)^{3/2} e^{-m_i/T_{X,\phi}}. \quad (\text{A4})$$

Given the fact that $m_X > T_{X,\phi} > m_\phi$, we have

$$a \equiv \frac{\Delta n_X}{\Delta n_\phi} \Big|_{T_{X,\phi}} = 12 e^{-m_X/T_{X,\phi}} \frac{g_X \mu_X}{g_\phi \mu_\phi} \left(\frac{m_X}{2\pi T_{X,\phi}}\right)^{3/2} = 12 e^{-m_X/T_{X,\phi}} \left(\frac{m_X}{2\pi T_{X,\phi}}\right)^{3/2}. \quad (\text{A5})$$

Assuming the symmetric component of X is annihilated completely and ϕ 's are too light to contribute significantly to the DM energy density, then we need $a \sim 10^{-3}$ to obtain the correct relic abundance for TeV mass of X . This implies $m_X/T_{X,\phi} \sim 10$ from Eq. (A5).

To determine the required cross section, we compare the interaction rate with Hubble,

$$\frac{n_X \sigma v}{H} \Big|_{T_{X,\phi}} \simeq 1 \quad (\text{A6})$$

The cross section of $X + X \rightarrow 2\phi + \phi^*$ is calculated as Eq. (A2). For $T < m_X$, $n_X = g_X \left(\frac{m_X T}{2\pi}\right)^{3/2} \exp[-(m_X - \mu_X)/T]$, $H = 1.66 \sqrt{g_*} T^2/M_{pl}$. Taking $m_X = 5$ TeV as an example, to satisfy Eq. (A6), one needs $y^2 \lambda^2 \sim 10^{-4}$, which is a reasonable choice of parameters with $y \sim \eta \sim 0.1$.

-
- [1] P. Hut, K. A. Olive, Phys. Lett. **B87**, 144-146 (1979).
 - [2] S. Nussinov, Phys. Lett. **B165**, 55 (1985).
 - [3] S. Dodelson, L. M. Widrow, Phys. Rev. **D42**, 326-342 (1990).
 - [4] G. B. Gelmini, L. J. Hall and M. J. Lin, Nucl. Phys. B **281**, 726 (1987).
 - [5] S. M. Barr, R. S. Chivukula, E. Farhi, Phys. Lett. **B241**, 387-391 (1990).
 - [6] S. M. Barr, Phys. Rev. **D44**, 3062-3066 (1991).
 - [7] D. B. Kaplan, Phys. Rev. Lett. **68**, 741-743 (1992).
 - [8] V. A. Kuzmin, Phys. Part. Nucl. **29**, 257-265 (1998). [hep-ph/9701269].
 - [9] D. E. Kaplan, M. A. Luty, K. M. Zurek, Phys. Rev. **D79**, 115016 (2009). [0901.4117 [hep-ph]].
 - [10] K. M. Zurek, arXiv:1308.0338 [hep-ph].

- [11] K. Petraki and R. R. Volkas, *Int. J. Mod. Phys. A* **28**, 1330028 (2013) [arXiv:1305.4939 [hep-ph]].
- [12] Y. Cai, M. A. Luty and D. E. Kaplan, arXiv:0909.5499 [hep-ph].
- [13] J. Shelton, K. M. Zurek, *Phys. Rev.* **D82**, 123512 (2010). [1008.1997 [hep-ph]].
- [14] N. Haba and S. Matsumoto, *Prog. Theor. Phys.* **125**, 1311 (2011) [arXiv:1008.2487 [hep-ph]].
- [15] J. McDonald, *Phys. Rev. D* **83**, 083509 (2011) [arXiv:1009.3227 [hep-ph]].
- [16] A. Falkowski, J. T. Ruderman, T. Volansky, *JHEP* **1105**, 106 (2011), [1101.4936 [hep-ph]].
- [17] G. R. Farrar, G. Zaharijas, *Phys. Rev. Lett.* **96**, 041302 (2006). [hep-ph/0510079].
- [18] P. -H. Gu, *Phys. Lett.* **B657**, 103-106 (2007). [0706.1946 [hep-ph]].
- [19] P. -H. Gu, U. Sarkar, X. Zhang, *Phys. Rev.* **D80**, 076003 (2009). [0906.3103 [hep-ph]].
- [20] H. An, S. -L. Chen, R. N. Mohapatra, Y. Zhang, *JHEP* **1003**, 124 (2010). [0911.4463 [hep-ph]];
- [21] H. An, S. -L. Chen, R. N. Mohapatra, S. Nussinov, Y. Zhang, *Phys. Rev.* **D82**, 023533 (2010). [1004.3296 [hep-ph]].
- [22] P. -H. Gu, M. Lindner, U. Sarkar and X. Zhang, *Phys. Rev. D* **83**, 055008 (2011) [arXiv:1009.2690 [hep-ph]].
- [23] L. J. Hall, J. March-Russell, S. M. West, [1010.0245 [hep-ph]].
- [24] D. E. Kaplan, G. Z. Krnjaic, K. R. Rehermann and C. M. Wells, *JCAP* **1110**, 011 (2011) [arXiv:1105.2073 [hep-ph]].
- [25] N. F. Bell, K. Petraki, I. M. Shoemaker and R. R. Volkas, *Phys. Rev. D* **84**, 123505 (2011) [arXiv:1105.3730 [hep-ph]].
- [26] C. Cheung and K. M. Zurek, *Phys. Rev. D* **84**, 035007 (2011) [arXiv:1105.4612 [hep-ph]].
- [27] J. March-Russell and M. McCullough, *JCAP* **1203**, 019 (2012) [arXiv:1106.4319 [hep-ph]].
- [28] M. L. Graesser, I. M. Shoemaker and L. Vecchi, arXiv:1107.2666 [hep-ph].
- [29] H. Davoudiasl, D. E. Morrissey, K. Sigurdson and S. Tulin, *Phys. Rev. Lett.* **105**, 211304 (2010) [arXiv:1008.2399 [hep-ph]].
- [30] H. Davoudiasl, D. E. Morrissey, K. Sigurdson and S. Tulin, *Phys. Rev. D* **84**, 096008 (2011) [arXiv:1106.4320 [hep-ph]].
- [31] N. Blinov, D. E. Morrissey, K. Sigurdson and S. Tulin, *Phys. Rev. D* **86**, 095021 (2012)

- [arXiv:1206.3304 [hep-ph]].
- [32] J. Huang and Y. Zhao, arXiv:1312.0011 [hep-ph].
- [33] Y. -Z. Fan, B. Zhang and J. Chang, Int. J. Mod. Phys. D **19**, 2011 (2010) [arXiv:1008.4646 [astro-ph.HE]].
- [34] A. Arvanitaki, S. Dimopoulos, S. Dubovsky, P. W. Graham, R. Harnik and S. Rajendran, Phys. Rev. D **79**, 105022 (2009) [arXiv:0812.2075 [hep-ph]].
- [35] E. Nardi, F. Sannino and A. Strumia, JCAP **0901**, 043 (2009) [arXiv:0811.4153 [hep-ph]].
- [36] S. Chang and L. Goodenough, Phys. Rev. D **84**, 023524 (2011) [arXiv:1105.3976 [hep-ph]].
- [37] I. Masina and F. Sannino, JCAP **1109**, 021 (2011) [arXiv:1106.3353 [hep-ph]].
- [38] I. Masina and F. Sannino, Phys. Rev. D **87**, 123003 (2013) [arXiv:1304.2800 [hep-ph]].
- [39] L. Feng and Z. Kang, JCAP **1310**, 008 (2013) [arXiv:1304.7492 [hep-ph]].
- [40] I. Masina, P. Panci and F. Sannino, arXiv:1205.5918 [astro-ph.CO].
- [41] B. Feldstein and A. L. Fitzpatrick, JCAP **1009**, 005 (2010) [arXiv:1003.5662 [hep-ph]].
- [42] S. D. Thomas, Phys. Lett. B **356**, 256 (1995) [hep-ph/9506274].
- [43] R. Kitano, I. Low, Phys. Rev. **D71**, 023510 (2005). [hep-ph/0411133].
- [44] J. Unwin, JHEP **1306**, 090 (2013) [arXiv:1212.1425 [hep-ph]].
- [45] J. J. Heckman and S. -J. Rey, JHEP **1106**, 120 (2011) [arXiv:1102.5346 [hep-th]].
- [46] [Fermi-LAT Collaboration], Astrophys. J. **750**, 3 (2012) [arXiv:1202.4039 [astro-ph.HE]].
- [47] M. Ackermann *et al.* [LAT Collaboration], Phys. Rev. D **86**, 022002 (2012) [arXiv:1205.2739 [astro-ph.HE]].
- [48] A. A. Abdo *et al.* [Fermi-LAT Collaboration], Phys. Rev. Lett. **104**, 101101 (2010) [arXiv:1002.3603 [astro-ph.HE]].
- [49] M. Cirelli, G. Corcella, A. Hektor, G. Hutsi, M. Kadastik, P. Panci, M. Raidal and F. Sala *et al.*, JCAP **1103**, 051 (2011) [Erratum-ibid. **1210**, E01 (2012)] [arXiv:1012.4515 [hep-ph], arXiv:1012.4515 [hep-ph]].
- [50] O. Adriani *et al.* [PAMELA Collaboration], Nature **458**, 607 (2009) [arXiv:0810.4995 [astro-ph]].
- [51] M. Aguilar *et al.* [AMS Collaboration], Phys. Rev. Lett. **110**, no. 14, 141102 (2013).
- [52] F. Aharonian *et al.* [H.E.S.S. Collaboration], Phys. Rev. Lett. **101**, 261104 (2008)

- [arXiv:0811.3894 [astro-ph]].
- [53] F. Aharonian *et al.* [H.E.S.S. Collaboration], *Astron. Astrophys.* **508**, 561 (2009)
[arXiv:0905.0105 [astro-ph.HE]].
- [54] I. V. Moskalenko and A. W. Strong, *Phys. Rev. D* **60**, 063003 (1999) [astro-ph/9905283].
- [55] I. V. Moskalenko and A. W. Strong, *Astrophys. J.* **493**, 694 (1998) [astro-ph/9710124].
- [56] E. A. Baltz and J. Edsjo, *Phys. Rev. D* **59**, 023511 (1998) [astro-ph/9808243].
- [57] AMS Collaboration,
<http://www.ams02.org/2013/07/new-ams-data-1-proton-spectrum-from-1-gv-to-1-8-tv/>
- [58] O. Adriani *et al.* [PAMELA Collaboration], *Phys. Rev. Lett.* **105**, 121101 (2010)
[arXiv:1007.0821 [astro-ph.HE]].
- [59] O. Adriani *et al.* [PAMELA Collaboration], *Science* **332**, 69 (2011) [arXiv:1103.4055
[astro-ph.HE]].
- [60] I. -W. Kim and K. M. Zurek, arXiv:1310.2617 [hep-ph].